Saliency performance investigation of Synchronous Machines for Position Sensorless Controlled EV drives

W.T. Villet*, M.H.A Prins†, C.W. Vorster‡, M.J. Kamper§
Department of Electrical and Electronic Engineering
Stellenbosch University
Stellenbosch, South Africa
*15053830@sun.ac.za, †mhaprins@sun.ac.za, ‡14827891@sun.ac.za, §kamper@sun.ac.za

***Abstract*—In this paper a per unit scale saliency- and saliency shift equation are used to predict the saliency based position sensorless control performance of synchronous machines for EV drives by means of a finite element package. These equations are used in a comparative study of various types of synchronous machines. The machine drives investigated and compared are a reluctance synchronous machine (RSM) hybrid EV drive and two variable gear RSM EV drives. Also included in the investigation are two field intensified permanent magnet (FI-PM) EV drives with asymmetric rotors, one FI-PM machine with a symmetric rotor and one field weakening interior permanent magnet drive. The saliency shift of the different FI-PM machine rotor topologies are also investigated. Closed loop saliency based position sensorless control shows startup torque capabilities of up to 304 Nm of a 32 kW 6-pole RSM. The RSM EV machine is used to investigate possible design modifications to improve on the saliency ratio and shift of synchronous machines.**

***Index Terms*—Position sensorless control, EV drives.**

NOMENCLATURE AND DEFINITIONS

Symbols:

u, i, ψ	Voltage current and flux linkage
r, L	Resistance and inductance
T_m, Θ	Mechanical torque and inertia
T_{ripple}	Torque ripple
f	Machine frequency
ϕ	Current angle
θ_r, ω_r	Rotor- angle and speed
θ_e, ω_e	Electrical- rotor angle and speed
Δ, Σ	Difference and sum

Indices:

s, r	Stator and rotor
α, β	Stator fixed cartesian axes
d, q	Rotor fixed direct and quadrature axes
c	Carrier frequency

Scalar values are written in normal letters, e.g. R or τ, vector values are written in small bold letters, e.g. $\boldsymbol{i}$ or $\boldsymbol{\psi}$. Subscripts describe the location of the physical quantity, e.g. r_s is the stator resistance. Superscripts specify the reference frame of the quantity, e.g. $\boldsymbol{i}_s^r$ is the stator current vector in the rotor reference frame. Estimated quantities are indicted with a hat, e.g. $\hat{\theta}_e$. Small signal values are represented with δ.

I. INTRODUCTION

Efficiency of electric- (EVs) and hybrid electric vehicles (HEVs) are enjoying increased research attention. It is shown in [1] and [2] that EVs with a variable gear (VG) drivetrain operate more efficiently on a drive cycle efficiency map than fixed gear (FG) EVs. One advantage of an EV with a VG drivetrain is the possibility of a downsized motor. Also machines with inadequate constant power speed range performance can be considered.

The reluctance synchronous machine (RSM) is a brushless machine without permanent magnets (PMs). Research has shown that the RSM drive is comparably efficient when compared to the induction machine [3], [4]. This machine however, has a limited constant power speed range in the field weakening area, hence this machine is ideal for a VG drivertrain EV.

The field intensified permanent magnet (FI-PM) machine does have sufficient constant power speed range performance for a FG EV drivetrain. Another machine with good constant power speed range performance is the field weakening interior permanent magnet (FW-IPM) machine which is a popular choice for FG EV drivetrains. It is reported in [5] that the magnet size of the FI-PM machine is 70% less than that of a FW-IPM machine. Along with the reduction in PM material it will also be possible to reduce the size of the FI-PM machine when used with a VG drivetrain EV.

It is still unsure whether completely position sensorless EV drives will be adopted by the industry. It is possible that position sensorless control might be used as backup to a position sensor. Saliency based position sensorless control methods are used at standstill and low speeds for position sensorless control of synchronous machines. It is shown in [6] and [7] however, that there are certain problems and limitations when the saliency is used for position sensorless control under loaded conditions. Saturation within the machine causes the magnitude of the saliency to decrease up to the point where position sensorless control is not possible any longer. Not only does the magnitude of the saliency decrease, but the magnetic axis is shifted away from the rotor axis when the machine

is loaded [8], [9]. It is found in [10] that this is caused by asymmetrical saturation of the rotor which increases the mutual inductance.

Although saliency based position sensorless control methods are only used at standstill and low speeds, it is important to investigate their limitations. Standstill-, or pull-away torque, is very important for electrical vehicles (EVs), thus it is important to be able to produce high torque at standstill. It is shown in [5] and [11] that the saliency of the FI-PM machine increases with increasing load, making it attractive for saliency based position sensorless control at standstill. The saliency based position sensorless control performance of the FI-PM machine however, is yet to be compared to that of a RSM which also have favorable characteristics for saliency based position sensorless control.

The rotors of electric machines are skewed to reduce the torque ripple. The rotor of the RSM only consists out of laminated steel, thus the process of skewing a RSM rotor is no more complex than that of an induction machine rotor. Skewing of the FI-PM machine on the other hand can increase manufacturing complexity. An alternative method of torque ripple reduction is proposed in [12] and [13] where the rotor of a RSM, a PM assisted RSM and an IPM machine are designed asymmetric to the reduce torque ripple. This rotor design is referred to as a butterfly rotor in [12].

In this paper a finite element (FE) package is used to predict the position sensorless control performance of EV drives on a per unit scale . The saliency based position sensorless control performance of the RSMs is compared to that of the FI-PM machines and the FW-IPM machine. Similar investigations are performed in [14] and [15] where individual machines are investigated without comparison to other types of machines. Also highlighted in this work is the saliency shift of different FI-PM machine rotor structures with and without asymmetric rotors. To aid investigations a 17 kW RSM drive, which was used in a HEV in [16], is used to compare the FE predicted saliency performance to the measured saliency performance.

II. Saliency ratio and saliency shift

The incremental inductances of the RSM are as defined in (1). These inductances are different to the absolute inductances and vary as a function of i_d and i_q [9]. According to [8] it can be assumed that the mutual inductances, which are caused by cross-saturation, are the same. Hence the mutual inductances are as in (2).

$$L_d = \frac{\partial \psi_d}{\partial i_d} \quad ; \quad L_q = \frac{\partial \psi_q}{\partial i_q} \tag{1}$$

$$\begin{cases} \psi_d = \psi_d(i_d, i_q), \\ \psi_q = \psi_q(i_d, i_q), \end{cases} \qquad \frac{\partial \psi_d}{\partial i_q} = \frac{\partial \psi_q}{\partial i_d} = L_{dq} = L_{qd} \tag{2}$$

It is shown in [8] that the linear relationship between flux linkage, inductance and current for the RSM can be represented by:

$$\delta \boldsymbol{\psi}_s^r = \begin{bmatrix} L_d & L_{dq} \\ L_{qd} & L_q \end{bmatrix} \delta \boldsymbol{i}_s^r \tag{3}$$

The small-signal current and flux vectors are represented by $\delta \boldsymbol{i}_s^r$ and $\delta \boldsymbol{\psi}_s^r$ respectively, as well as the column matrices in (3). The small signal currents are thus described as in (4) and (5) [17].

$$\delta i_d = \frac{L_q \delta \psi_d + L_{dq} \delta \psi_q}{L_d L_q - L_{dq}^2} \tag{4}$$

$$\delta i_q = \frac{L_d \delta \psi_q - L_{dq} \delta \psi_d}{L_d L_q - L_{dq}^2} \tag{5}$$

When the alternating high frequency injection position sensorless control method is considered, the RSM can be described electrically by (6). Equation (6) is only valid when the injection frequency is high enough. The HF voltage is as in (7).

$$\boldsymbol{u}_s^r = \boldsymbol{L}^r \frac{d}{dt} \boldsymbol{i}_s^r \tag{6}$$

$$\boldsymbol{u}_s^r = \begin{bmatrix} u_c cos(\omega_c t) \\ 0 \end{bmatrix} \tag{7}$$

The resulting flux linkage can be written as in (8) according to [8] and [17]. The small signal current response is thus rewritten as in (9) [8].

$$\delta \psi_d = \frac{u_c}{\omega_c} cos(\omega_c t) \tag{8}$$

$$\delta i_s^r = \frac{u_c sin(\omega_c t)}{\omega_c} \left[\frac{\Sigma L}{L_d L_q - L_{dq}^2} - \left(\sqrt{\left(\frac{\Delta L}{L_d L_q - L_{dq}^2} \right)^2 + \left(\frac{L_{dq}}{L_d L_q - L_{dq}^2} \right)^2} \right) e^{-j2\Delta\theta_e} \right] \tag{9}$$

where

$$\Delta L = \frac{L_d - L_q}{2} \tag{10}$$

$$\Sigma L = \frac{L_d + L_q}{2} \tag{11}$$

It is stated by [8], [9] and [17] that, due to the mutual inductance, the negative sequence component of (9) (which is used in the demodulation process) is rotated by an angle γ. This angular offset is known as the saliency shift and can be calculated as in (12) [8], [9], [17].

$$\gamma = -0.5 \arctan\left(\frac{L_{dq}}{\Delta L} \right) \tag{12}$$

As stated by [9], the saliency shift will be zero at no load or if the geometric saliency is dominant enough to mask the effect

of the saturation saliency. This then prevents the magnetic axis from moving away from the rotor d-axis [9]. It is possible to compensate for the saliency shift within the control, if the saliency shift of the machine is known.

Although the mutual inductance causes a shift of the magnetic axis, it also contributes to the magnitude of the saliency [9]. This terms should thus be taken into account when calculating the saliency of the machine. The saliency ratio is defined in [8] as the ratio of the negative sequence amplitude over the positive sequence amplitude. The saliency ratio equation is as in (13) [8], [9]. The saliency ratio is thus a parameter greater than zero that allows the machine saliency to be characterised on a per unit scale. Larger saliency ratio values are considered better for saliency based position sensorless control, but the effectiveness of the saliency based position sensorless controllability also depends on the saliency shift.

$$\zeta = \frac{\sqrt{(L_d - L_q)^2 + 4L_{dq}^2}}{L_d + L_q} \tag{13}$$

III. Saliency performance of a HEV RSM drive

A 17 kW RSM drive, which is used in a HEV in [16], is evaluated in the JMAG FE package. The geometry of this machine is as shown in Fig. 1. The specifications of this machine are summarised in Table I as drive 1. The saliency ratio and saliency shift of this machine are calculated with JMAG at various operating points on the maximum torque per ampere current angle curve with equations (12) and (13). The saliency ratio and saliency shift of the RSM is also measured to verify the FE results. The evaluated RSM is connected via a torque sensor to an induction machine on a tests bench. Two rapid prototype system, as shown in Fig. 2 are used to control two DC linked connected inverters, one for each machine.

The measured results are shown in Fig. 3. There is a saliency ratio measurement error of 6%, which is acceptable. The saliency shift however, does not correlate well. This is due to the small mutual inductance term which is difficult to measure.

It is shown in Fig. 3 that the saliency ratio of the RSM climbs quite steeply as the current increases and then steadily declines as the machine approaches rated current while the

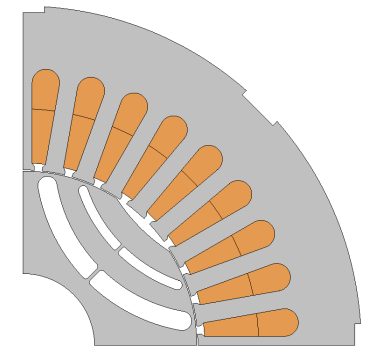

Fig. 1: Geometry of machine 1.

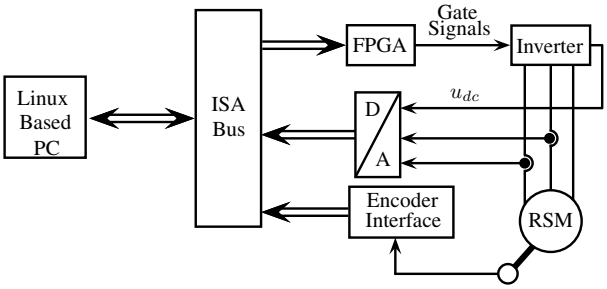

Fig. 2: Rapid prototype system used with test bench.

absolute value of the saliency shift increases non-linearly. The correlations between the measured and simulated saliency ratio suggest that the FE simulations are accurate enough to predict the saliency performance of a machine before it is manufactured. It also shows that the RSM has favourable characteristics for saliency based position sensorless control.

IV. Variable gearbox EV drive

The first considered EV drive is aimed at a small commercial vehicle. The specifications of an Opel Corsa vehicle are used to simulate, design and build a RSM to replace its internal combustion engine and operate with its stock gearbox. The Opel Corsa used is shown in Fig. 4. The specifications of this machine are summarised in Table I as drive 2. Machine 2 has chorded stator windings and a skewed rotor to reduce the torque ripple. This machine's geometry is shown in Fig. 5a.

The third RSM drive used in this investigation has 6 poles. This machine can be used to replace the internal combustion diesel engine of a tractor, small pick-up or even a small marine diesel engine with a VG. This machine is not skewed, but have chorded stator windings. The specifications of this machine are given in Table I as machine 3. The geometry of this machine is as in Fig. 5b.

Machines 4, 5 & 6 are FI-PM machines. The investigated FI-PM machines are also designed to the specifications of the

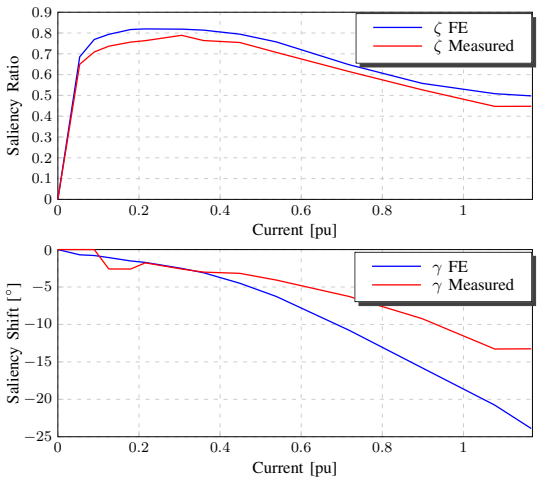

Fig. 3: Measured and simulated saliency ratio and saliency shift of machine 1.

VG drivetrain of the Opel Corsa, although the FI-PM machines will also perform well in a FG EV drivetrain. The results summary of the FI-PM machines in Table I show that the asymmetric rotor configuration as well as the stator cording are effective in reducing the torque ripple.

Machine 4 is a surface mounted FI-PM machine as shown in Fig. 6a. Machine 5 is a field intensified interior permanent magnet (FI-IPM) machine with its magnet buried into the rotor as shown in Fig. 6b. It is shown in Fig. 6 that both machines 4 and 5 are simulated as half models instead of quarter models as in Fig. 5 due to their asymmetrical butterfly rotors.

The third FI-PM machine also has its magnet buried in the rotor. This machine however, as shown in Fig. 6c, have barriers on the q-axis similar to that of a RSM. This rotor however, is symmetrical, hence is only simulated as a quarter model. For comparison a FW-IPM machine, which is designed for a fixed gear drivetrain EV, is included as drive 7. This machine is shown in Fig. 6d.

V. FE EVALUATION OF THE INVESTIGATED EV DRIVES

The seven drives, as summarised in Table I, are simulated in the JMAG FE package in order to investigate each machine's saliency ratio- and saliency shift performance at its maximum torque per ampere current angle, ϕ. These results are shown in Figs. 7 and 8. The three RSM drives (1-3) all have a large saliency ratio throughout their rated current region as seen in Fig. 7. The saliency of all three FI-PM machines (4-6) start low in comparison to that of the RSM and increase steadily as the current increases. The saliency ratio of the FI-PM machines at rated current, however are still lower than that of the RSM. The saliency ratio of the three FI-PM machines should still be large enough at rated current for saliency based position sensorless control.

The surface mounted FI-PM machine however, has a large region in its low current region where its saliency ratio is very small. Inverter non-linearities, system noise and limited bandwidth might thus prevent successful saliency based position sensorless control in this region. In contrast to the increasing saliency ratio of the FI-PM machines, the FW-IPM machines' saliency ratio decreases drastically as the current increase. Saliency based position sensorless control of the FW-IPM will thus not be possible at rated current.

Fig. 4: Opel Corsa used for the EV application.

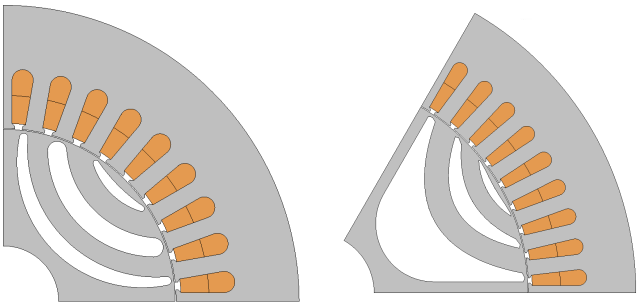

(a) Machine 2 (b) Machine 3

Fig. 5: Two RSM drives considered for VG EV drive applications.

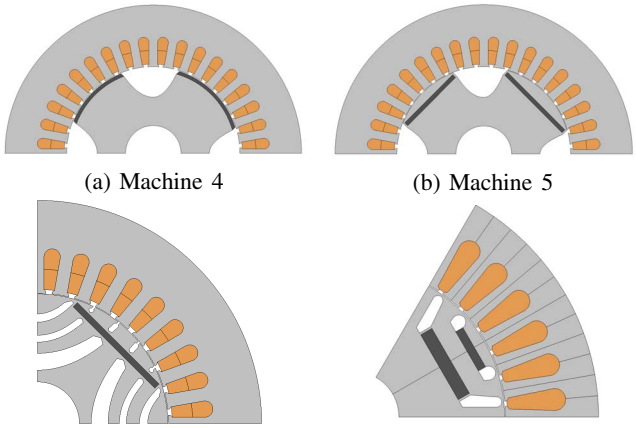

(a) Machine 4 (b) Machine 5

(c) Machine 6 (d) Machine 7

Fig. 6: Four PM machines considered for EV drive applications.

TABLE I: Evaluated EV drives

Drive #	Machine	Rotor	Windings	f [Hz]	i_{rms} [A]	ϕ [degrees]	P [kW]	T_{ripple} [%]
1	RSM	Skewed	Chorded: 7/9	90	39.39	67^o	17	6.4
2	RSM	Skewed	Chorded: 7/9	160	139	67^o	35	6.9
3	RSM 6-pole	Unskewed	Chorded: 7/9	50	62.4	64^o	31.8	13.5
4	FI-PM-Surface	Butterfly	Chorded 8/9	160	143	71^o	41.3	8.8
5	FI-IPM	Butterfly	Chorded 7/9	160	143	71^o	32.1	6.6
6	FI-IPM-Barriers	Unskewed	Chorded 8/9	160	143	86^o	34.1	14
7	FW-IPM	Skewed 2 Stacks	Not chorded 9/9	114.5	223	143^o	54	12.6

It is shown in Fig. 8 that machines 4 and 5 suffer from a significant saliency shift. This might be due to the rotor geometry of these FI-PM machines which doesn't have flux barriers to constraints the flux within definite paths. The saliency shift of the FW-IPM machine is also fairly large at large current magnitudes. It is clear that the sign of the saliency shift of the FW-IPM changes direction when the gradient of its saliency ratio changes sign at 0.9 pu. Finally, it is shown in Fig. 8 that all three RSMs and the barrier FI-IPM machine have got minimal saliency shift.

VI. Measured analysis of the RSM EV drive

FE results of machine 2 indicates that this machine will perform well with saliency based position sensorless control. The saliency ratio of machine 2 is measured on the test bench described in the previous section and compared to its FE results. Due to this machine's very high current rating no drive was available to test this machine up to rated load, but measured results up to 0.6 p.u correlate well with the FE results, and thus it can be assumed that the FE results are accurate up to rated load. These results are shown in Fig. 9.

VII. Closed Loop Saliency Based Position Sensorless Control of Machine 3

It is important to verify the FE results with proper closed loop saliency based position sensorless control. Machine 3 will be used for this purpose. At 304 Nm this machine can deliver the highest torque of all 7 evaluated machines. Two position sensorless control methods are used namely an alternating high frequency injection- and an arbitrary injection method [18], [19].

The first set of tests is the locked rotor test. A disc brake is used to lock the rotor of the RSM while the current is ramped up to rated current. The current is measured, transformed to the actual rotary reference with the measured electrical angle of the machine and saved. This current vector is not used in the feedback loop, but rather used offline to calculate the torque produced by the machine by means of a lookup table created from the FE package. The current vector in the estimated rotary reference frame, which is used in the feedback loop, might produce inaccurate results.

The locked rotor results of machine 3 with the alternating high frequency injection position sensorless control method are shown in Fig. 10 and the results of the arbitrary injection method in Fig. 11. The torque ripple in Fig. 10 at 1.4 s is the result of the disc brake slipping causing the rotor to turn one revolution inducing a large position estimation error momentarily. The locked rotor test is done at various different rotor positions. Figs. 10 and 11 show that both methods can deliver rated torque at standstill.

The position estimation error, θ_{error} in Figs. 10 and 11 is in electrical degrees. It is clear that the position estimation error never surpasses 20^o.

The second test is a steady state test at a low speed setpoint. Machine 3 is loaded by a load machine while in speed control. Again both the HF injection and arbitrary injection methods

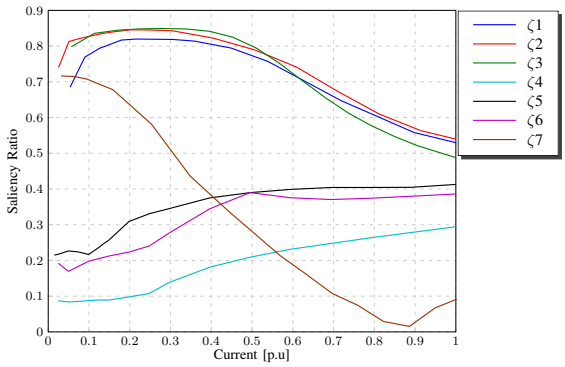

Fig. 7: Simulated saliency ratio comparison.

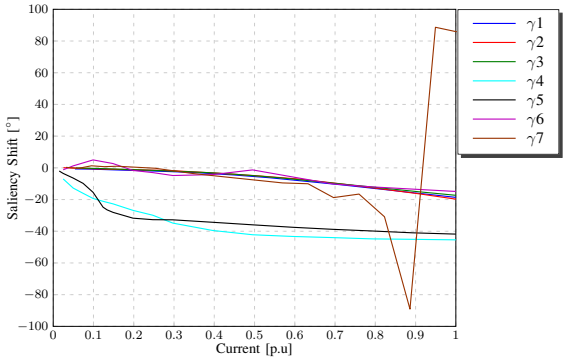

Fig. 8: Simulated saliency shift comparison.

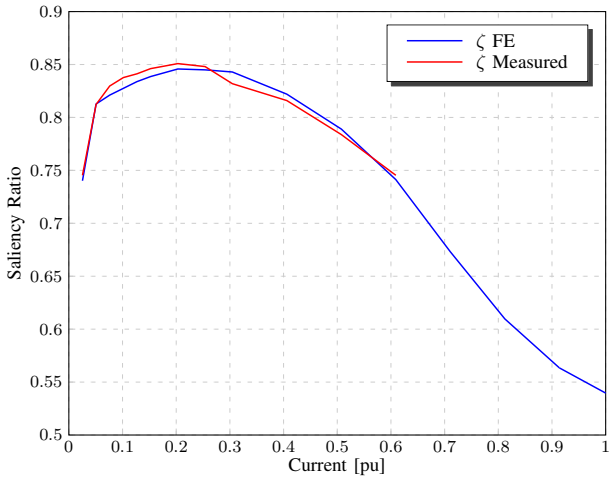

Fig. 9: Measured and simulated saliency ratio of machine 2.

are used for saliency based position sensorless control. The results of this test are shown in Figs. 12 and 13. Again, the current in the real rotor reference frame is used offline with a torque lookup table to determine the torque applied by the machine. The torque ripple seen in Fig. 12 is a result of an unbalanced shaft connection between the two machines that exists at certain frequencies. The speed controller thus rectifies

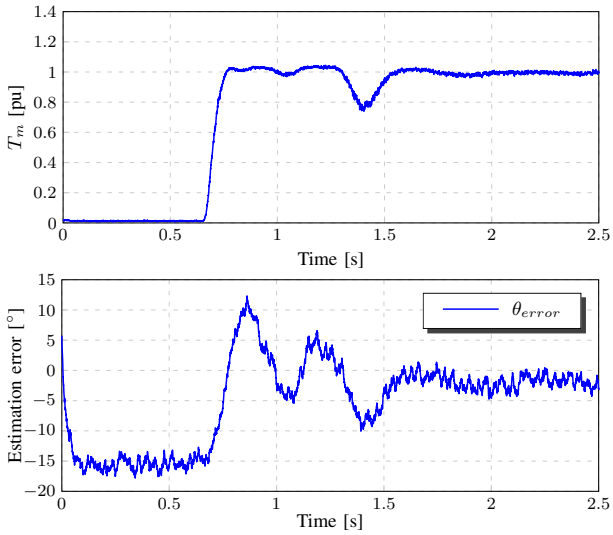

Fig. 10: Locked rotor test on machine 3 with the HF injection method.

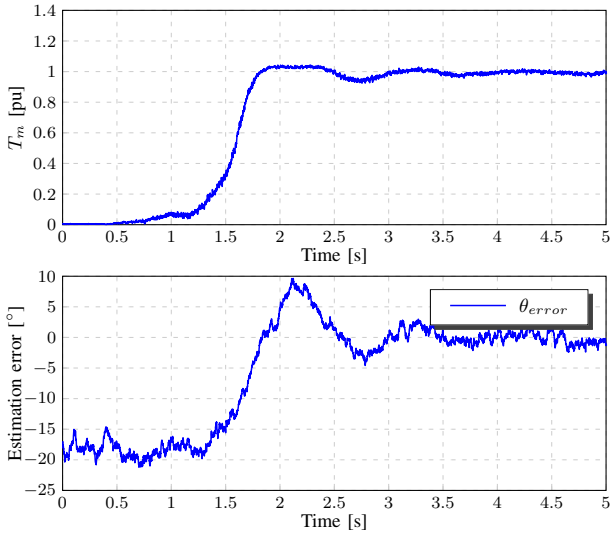

Fig. 11: Locked rotor test on machine 3 with the arbitrary injection method.

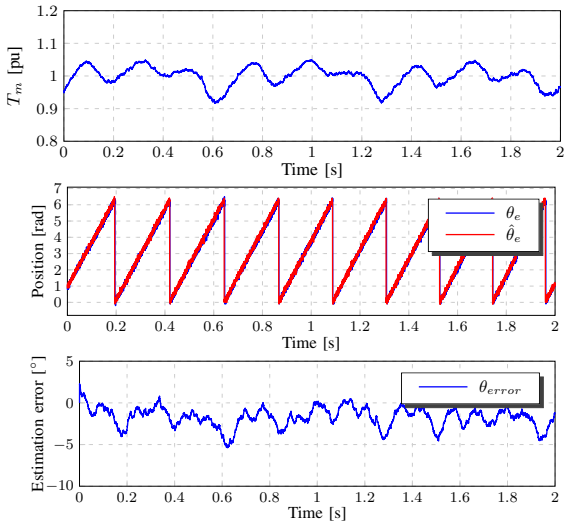

Fig. 12: Steady state test on machine 3 with the HF injection method.

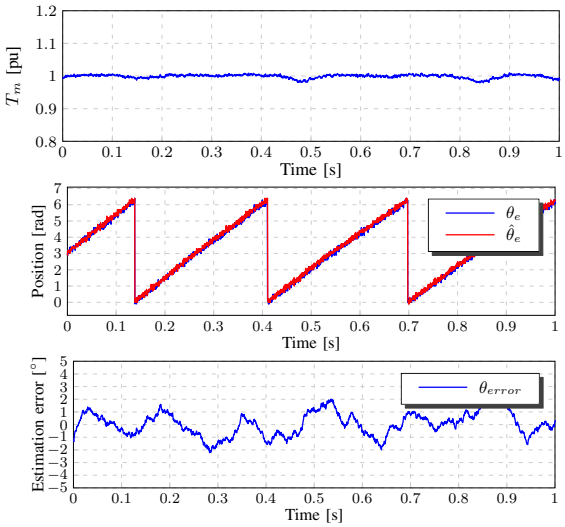

Fig. 13: Steady state test on machine 3 with the arbitrary injection method.

this ripple causing the torque to ripple. These results show that it is possible for machine 3 to deliver rated torque at low speeds with saliency based position sensorless control.

The two tests described above thus prove that stable saliency based position sensorless control is possible with a saliency ratio of 0.48 p.u and that it is possible to compensate for a saliency shift of $|18° |$.

VIII. Improving on the Saliency Ratio and -Shift

It is shown in the previous sections that it is possible to accurately predict the saliency ratio and -shift of synchronous machines by means of FE simulations. It thus makes sense to exploit the flexibility and comfort of FE software to determine how to increase the saliency ratio and decrease the saliency shift of synchronous machines.

It is found in [20] that to increase the saliency ratio of PM machines the tooth width of the stator should be decreased and the slot opening width should be increased. It is also shown in [20] that the slot geometry is an effective saliency parameter. The author in [10] states that the d- and q-axis flux linkages are constraint in more definite paths when the rotor has a high number of flux barriers per pole, thus reducing the cross-coupling effect. The saliency shift is thus reduced when the cross-coupling between the magnetic d- and q-axis is reduced.

Machine 2 is used as a base model to investigate these effects. Machine 2 is modified in three different ways:

1) Increase the rotor flux barriers from 3 to 8.
2) Increase slot opening width from $2.53°$ to $4.234°$.
3) Increase the rotor flux barriers from 3 to 8 and increase the slot opening width from $2.53°$ to $4.234°$.

The FE results of the three described experimental modifications are summarised in Table II. The aim of the machine modifications are to increase the saliency ratio, ζ, and to decrease the absolute value of the saliency shift, γ. The torque ripple is also evaluated to determine how the modifications affect the power quality of the machine. None of these machines, including the base machine, are simulated with skewed rotors. It should be noted, however, that the base model (machine 2) is optimised for maximum torque and minimum torque ripple. This optimisation process is not applied to the three modified designs. The torque of the based model is chosen as the 1 p.u to compare to the modified designs.

The results of modification 1 clearly show that the saliency shift decreases dramatically when the number of flux barriers per pole are increased. The saliency ratio, however also decreases by 6.94%. The results of modification 2 show that both the saliency ratio and the saliency shift improve when the slot opening width is increased. The results of modification 3 show that the saliency shift improves even further when the number of flux barriers per pole is increased as well as the slot opening width. This saliency shift improvement of modification 3 however, is slightly more than of modification 2 with a reduction in size of the saliency ratio. The increase in torque ripple of modification 3 is also significantly larger than the other two modifications. The simulated saliency ratio and -shift curves of the base model and modifications as a function of current are as shown in Fig. 14.

It is important to investigate if the machine modifications affect the power quality of the machine. The losses of the base model are compared to that of the modified designs in Table III. The rotor- and stator losses of the base model is chosen as the 1 $p.u$ value in this investigation. It is shown in Table III that iron loss in the stator of all three modified designs are lower than that of the base model. The iron losses in the rotor of the modified designs, however are higher. The rotor iron losses of modification 3 is more than twice that of the the base model. Proper optimisation methods. however might reduce the rotor losses.

IX. Conclusion

A saliency ratio equation is used to calculate the saliency of synchronous machines with different power ratings on a per-unit scale. Measurements of a HEV RSM drive are used to confirm that it is possible to accurately predict the saliency ratio of a machine with a FE package. Two RSMs for EV applications are considered. FE simulation results indicates that both machines are well suited for saliency based position sensorless control. The measured saliency ratio of the four pole RSM drive show accurate prediction of its saliency performance before manufacturing.

Closed loop saliency based position sensorless control of the 6 pole RSM show that 100% startup torque is achievable at a saliency ratio of 0.48 p.u and a saliency shift of $\mid 18° \mid$. The two methods of position sensorless control used are the alternating high frequency injection and the arbitrary injection position sensorless control method.

The saliency ratio simulation results of three FI-PM machines and a FW-IPM machine are compared to that of the RSMs. It is found that the saliency ratio of the RSM is higher than that of the FI-PM machines throughout the entire rated current region. It is also shown that the saliency ratio of the FW-IPM machine declines steeply as the current increases.

Simulation results show that the saliency ratio of the FI-PM machines increase with current, as expected. It is found however, that the FI-PM machine configuration with the magnet on the surface has a large region in it's low current region where saliency based position sensorless control might not be

TABLE II: Summarised simulated results of experimental modifications made to machine 3.

	ζ	$\mid\gamma\mid$	T_{ripple}
Base	53.66%	$18.56°$	13.92 %
Modification 1	$\downarrow$ 6.94%	$\downarrow$ $2.01°$	$\uparrow$ 3.97%
Modification 2	$\uparrow$ 4.68%	$\downarrow$ $4.61°$	$\uparrow$ 3.66%
Modification 3	$\downarrow$ 2.93%	$\downarrow$ $4.9°$	$\uparrow$ 8.78%

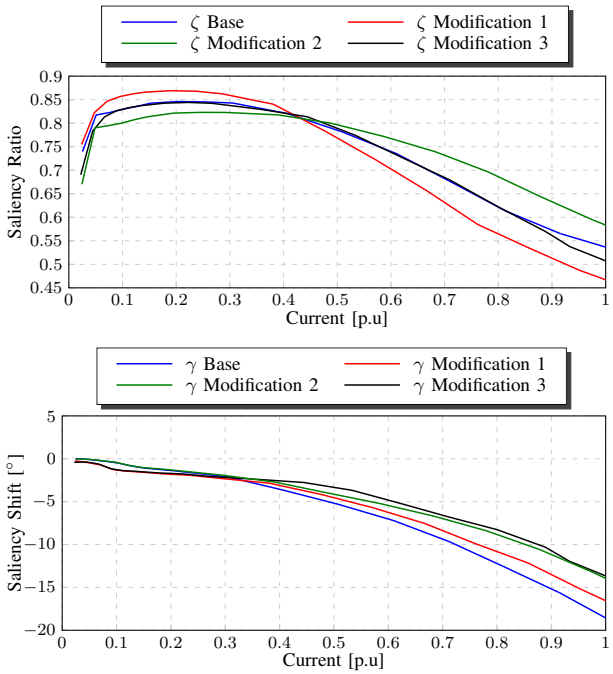

Fig. 14: FE results of machine modifications.

TABLE III: Comparison of losses obtained from FE.

	Rotor core [pu]	Stator core [pu]
Base	1	1
Modification 1	1.4	0.82
Modification 2	1.53	0.85
Modification 3	2.16	0.75

possible.

FE simulations shows that the saliency shift of the two FI-PM machines without flux barrier are significantly larger than that of the FI-IPM machine with flux barriers. It is shown that the saliency shift of the FI-IPM machine with barriers is smaller than the other two investigated FI-PM machines and correlates well with that of the investigated RSMs.

Furthermore it is shown that the saliency ratio of the RSM is reduced when the number of flux barriers per pole are increased. The saliency shift however, improves when the number of flux barriers per pole is increased. It is also shown that both the saliency ratio and -shift improve when the width of the stator slot opening is increased. It is also found that the torque ripple of the machine increases significantly when the number of flux barriers per pole is increased in conjunction with the stator slot opening.

The FE software is also used to investigate the effect of the rotor modifications on the iron losses. It is found that the stator iron losses are less with the modified designs, but the rotor losses are more. A redesign optimisation of the modified designs can reduce the rotor losses and decrease the torque ripple.

REFERENCES

[1] Q. Ren, D. Crolla, and A. Morris, "Effect of transmission design on electric vehicle (ev) performance," in *Vehicle Power and Propulsion Conference, 2009. VPPC '09. IEEE*, sept. 2009, pp. 1260 –1265.

[2] L. Lai and M. Ehsani, "Sensitivity analysis of vehicle performance to transmission parameters in parallel hevs with dynamic programming optimization," in *Transportation Electrification Conference and Expo (ITEC), 2012 IEEE*, june 2012, pp. 1 –5.

[3] J. Germishuizen, F. van der Merwe, K. Van der Westhuizen, and M. Kamper, "Performance comparison of reluctance synchronous and induction traction drives for electrical multiple units," in *Industry Applications Conference, 2000. Conference Record of the 2000 IEEE*, vol. 1, 2000, pp. 316 –323 vol.1.

[4] A. Boglietti, A. Cavagnino, M. Pastorelli, and A. Vagati, "Experimental comparison of induction and synchronous reluctance motors performance," in *Industry Applications Conference, 2005. Fourtieth IAS Annual Meeting. Conference Record of the 2005*, vol. 1, oct. 2005, pp. 474 – 479 Vol. 1.

[5] S. Wu, D. Reigosa, Y. Shibukawa, M. Leetmaa, R. Lorenz, and Y. Li, "Interior permanent-magnet synchronous motor design for improving self-sensing performance at very low speed," *Industry Applications, IEEE Transactions on*, vol. 45, no. 6, pp. 1939–1946, Nov.-dec.

[6] N. Bianchi and S. Bolognani, "Influence of rotor geometry of an interior pm motor on sensorless control feasibility," in *Industry Applications Conference, 2005. Fourtieth IAS Annual Meeting. Conference Record of the 2005*, vol. 4, oct. 2005, pp. 2553 – 2560 Vol. 4.

[7] N. Bianchi, S. Bolognani, J.-H. Jang, and S.-K. Sul, "Comparison of pm motor structures and sensorless control techniques for zero-speed rotor position detection," *Power Electronics, IEEE Transactions on*, vol. 22, no. 6, pp. 2466 –2475, nov. 2007.

[8] P. Guglielmi, M. Pastorelli, and A. Vagati, "Cross-saturation effects in ipm motors and related impact on sensorless control," *Industry Applications, IEEE Transactions on*, Nov.-dec. 2006.

[9] T. Frenzke, "Impacts of cross-saturation on sensorless control of surface permanent magnet synchronous motors," in *Power Electronics and Applications, 2005 European Conference on*.

[10] N. Bianchi, S. Bolognani, and M. Zigliotto, "Design hints of an ipm synchronous motor for an effective position sensorless control," in *Power Electronics Specialists Conference, 2005. PESC '05. IEEE 36th*, june 2005, pp. 1560 –1566.

[11] N. Limsuwan, Y. Shibukawa, D. Reigosa, and R. Lorenz, "Novel design of flux-intensifying interior permanent magnet synchronous machine suitable for self-sensing control at very low speed and power conversion," *Industry Applications, IEEE Transactions on*, vol. 47, no. 5, pp. 2004–2012, Sept.-Oct.

[12] N. Bianchi, S. Bolognani, D. Bon, and M. Pre, "Rotor flux-barrier design for torque ripple reduction in synchronous reluctance and pm-assisted synchronous reluctance motors," *Industry Applications, IEEE Transactions on*, vol. 45, no. 3, pp. 921–928, 2009.

[13] L. Alberti, M. Barcaro, and N. Bianchi, "Design of a low torque ripple fractional-slot interior permanent magnet motor," in *Energy Conversion Congress and Exposition (ECCE), 2012 IEEE*, Sept., pp. 509–516.

[14] M. Barcaro, A. Faggion, N. Bianchi, and S. Bolognani, "Predicted and experimental anisotropy of a dual three-phase interior permanent magnet motor for sensorless rotor position control," in *Power Electronics, Machines and Drives (PEMD 2012), 6th IET International Conference on*, 2012, pp. 1–6.

[15] N. Bianchi, S. Bolognani, A. Faggion, E. Fornasiero, and A. Sartorello, "Zero-speed sensorless drive capability of fractional-slot inset pm machine," in *Power Electronics, Machines and Drives (PEMD 2012), 6th IET International Conference on*, 2012, pp. 1–6.

[16] J. Malan and M. Kamper, "Performance of a hybrid electric vehicle using reluctance synchronous machine technology," *Industry Applications, IEEE Transactions on*, vol. 37, no. 5, pp. 1319–1324, Sep/Oct.

[17] N. Bianchi, E. Fornasiero, and S. Bolognani, "Effect of stator and rotor saturation on sensorless rotor position detection," *Industry Applications, IEEE Transactions on*, vol. 49, no. 3, pp. 1333–1342, 2013.

[18] W. T. Villet, M. Kamper, P. Landsmann, and R. Kennel, "Evaluation of a simplified high frequency injection position sensorless control method for reluctance synchronous machine drives," in *Power Electronics, Machines and Drives (PEMD 2012), 6th IET International Conference on*, 2012, pp. 1–6.

[19] D. Paulus, P. Landsmann, and R. Kennel, "Sensorless field- oriented control for permanent magnet synchronous machines with an arbitrary injection scheme and direct angle calculation," in *Sensorless Control for Electrical Drives (SLED), 2011 Symposium on*, 2011, pp. 41–46.

[20] M. Caner, C. Gerada, and G. Asher, "Permanent magnet motor design optimisation for sensorless control," in *Electrical Machines and Power Electronics and 2011 Electromotion Joint Conference (ACEMP), 2011 International Aegean Conference on*, 2011, pp. 670–675.